UCLA
UCLA Previously Published Works

Title

Diffusion microstructure alterations in subcortical gray matter are associated with cognitive and motor performance in Parkinson's disease: a pilot study

Permalink

https://escholarship.org/uc/item/8rm6g4sc

Journal

Frontiers in Neurology, 17

ISSN

1664-2295

Authors

Newman, Benjamin T
Foreman, Ryan
Donahue, Erin
et al.

Publication Date

2026-07-29

DOI

10.3389/fneur.2026.1863964

Copyright Information

This work is made available under the terms of a Creative Commons Attribution License, available at https://creativecommons.org/licenses/by/4.0/

Peer reviewed

eScholarship.org Powered by the California Digital Library
University of California

frontiers in Neurology

TYPE Original Research
PUBLISHED 29 July 2026
DOI 10.3389/fneur.2026.1863964

Check for updates

OPEN ACCESS

EDITED BY
Sergio Sebastia-Amat,
University of Alicante, Spain

REVIEWED BY
Minoo Sharbafshaaer,
University of Campania "Luigi Vanvitelli", Italy
Gilberto Perez Rodriguez Garcia,
Boston University, United States

*CORRESPONDENCE
John Darrell Van Horn
jdv7g@virginia.edu

RECEIVED 24 April 2026
REVISED 03 July 2026
ACCEPTED 08 July 2026
PUBLISHED 29 July 2026

CITATION
Newman BT, Foreman R, Donahue E, Jakowec MW, Petkus AJ, Holschneider DP, O'Neill J, Schiehser DM, Petzinger G and Van Horn JD (2026) Diffusion microstructure alterations in subcortical gray matter are associated with cognitive and motor performance in Parkinson's disease: a pilot study.
Front. Neurol. 17:1863964.
doi: 10.3389/fneur.2026.1863964

COPYRIGHT
© 2026 Newman, Foreman, Donahue, Jakowec, Petkus, Holschneider, O'Neill, Schiehser, Petzinger and Van Horn. This is an open-access article distributed under the terms of the Creative Commons Attribution License (CC BY). The use, distribution or reproduction in other forums is permitted, provided the original author(s) and the copyright owner(s) are credited and that the original publication in this journal is cited, in accordance with accepted academic practice. No use, distribution or reproduction is permitted which does not comply with these terms.

Diffusion microstructure alterations in subcortical gray matter are associated with cognitive and motor performance in Parkinson's disease: a pilot study

Benjamin T. Newman[1], Ryan Foreman[2], Erin Donahue[2], Michael W. Jakowec[2], Andrew J. Petkus[2], Daniel P. Holschneider[2], Joseph O'Neill[3], Dawn M. Schiehser[4,5], Giselle Petzinger[2] and John Darrell Van Horn[1,6]*

[1]Department of Psychology, University of Virginia, Charlottesville, VA, United States, [2]Department of Neurology, University of Southern California, Los Angeles, CA, United States, [3]Division of Child & Adolescent Psychiatry, Department of Psychiatry and Biobehavioral Sciences, University of California Los Angeles, Los Angeles, CA, United States, [4]Veterans Administration San Diego Healthcare System (VASDHS), San Diego, San Diego, CA, United States, [5]Department of Psychiatry, University of California, San Diego, San Diego, CA, United States, [6]School of Data Science, University of Virginia, Charlottesville, VA, United States

The cholinergic basal forebrain and subcortical gray matter have previously been implicated in Parkinson's disease (PD), but the relationship between the symptomology of PD, including cognitive impairment, and specific patterns of damage remains unclear. Additionally, understanding the impact of fitness, including motor skills, on brain structure remains a knowledge gap. In this study, we examine a longitudinal cohort of PD patients using advanced microstructural analysis derived from diffusion MRI, alongside volumetric and connectivity components. These imaging metrics are compared to comprehensive cognitive and motor skill fitness metrics. Although the volumetric components well characterize change across the longitudinal timescale, the microstructural analysis was related to a number of composite cognitive scores, including attention, executive function, cognition, language, and the level of motor skill fitness. We further assess the connectivity of the cholinergic basal forebrain, particularly the nucleus basalis of Meynert in area 4 (CH4), and find that connectivity between CH4 and the thalamus is associated with motor skill fitness. The pattern of microstructural results suggests that increased cellularity may support reduced cognitive decline in individuals with PD and greater motor skill fitness.

KEYWORDS
cognition, diffusion MRI, exercise, microstructure, Parkinson's disease, structural connectivity

Introduction

Alongside its well-known motor symptoms, wide-ranging cognitive deficits are common in Parkinson's disease (PD) (1, 2). Per Braak's staging hypothesis (3), PD develops gradually as a neurotoxic aggregate form of alpha-synuclein protein accumulates in structure after structure of the brain roughly in stages. As alpha-synuclein load rises and neurons perish in each region, symptoms emerge reflecting interference with the normal functions of the region and/or its efferent targets. Thus, the hallmark motor symptoms of PD stem primarily from loss of pigmented neurons in the substantia nigra pars compacta and consequent interruption of their dopamine (DA) projections to the caudate and putamen (4). Cognitive symptoms, the focus of this report, in contrast, have been partly attributed to synuclein pathology in the Ch4 portion of the nucleus basalis of Meynert in the substantia innominata and to interruption of their acetylcholine (ACh) supply to the amygdala and neocortex (5–7). Other segments of the cholinergic basal forebrain, including the medial septum (Ch1) and the vertical (Ch2) and horizontal (Ch3) limbs of the diagonal band of Broca, and their main target, the hippocampus, are similarly afflicted (3) (We refer below to the closely adjacent Ch1, Ch2, and Ch3 cholinergic centers collectively as "Ch123"). The Braaks' hypothesis implies that appropriate *in vivo* non-invasive neuroimaging of brain structures compromised by PD may aid clinicians and researchers in diagnosing and staging the disorder, making prognoses, identifying the anatomic sources of symptoms, and perhaps even designing novel therapies and predicting treatment outcomes.

These goals have been pursued intensively using magnetic resonance (MR) methods. Thereby, conventional morphometric structural MRI may prove too coarse to image small nuclei implicated in PD, such as Ch4 and Ch123, quantifiably and reliably (8, 9). Diffusion microstructure imaging, in contrast, affords higher resolution and greater detail than macroscopic volumetric measures in characterizing symptom-generating structural degradation in PD (10). Although still a surrogate for cellular changes, microstructural metrics can sample inside intra-axonal spaces, detect activated microglia and astrocytes, and measure changes in extracellular water content, such as those left by neuronal atrophy (11). A great deal of work has been focused on diffusion tensor imaging-based measures of microstructure due to the ease of calculation. For example, a prior study described widespread changes in fractional anisotropy (FA) using tract-based spatial statistics in PD patients with psychosis compared to PD patients without psychosis (12). Another study similarly found changes in FA associated with cognitive and executive function deficits with these associations being located in different segments of WM tracts depending on the cognitive process being assessed, further demonstrating that different symptom profiles may arise from different neurological patterns of damage (13). Microstructural differences in FA have been observed between PD patients with cognitive impairment and those without, even in the absence of macrostructural, cortical thickness, or volumetric differences (14). Other studies using more advanced microstructural models have sought to more closely link imaging metrics with underlying cellular changes. For example, studies have reported increased extracellular free water in the substantia nigra in PD patients, indicating neuroinflammation or atrophy (11, 15).

This detail provided by microstructural analysis is important, not only for well-characterizing neuronal structure in PD but also to explore the involvement of additional cellular types, which may represent new treatment targets. A series of studies in mouse models has suggested that glial markers, particularly astrocytic markers, are active in PD (16, 17). The above-mentioned capacity of diffusion microstructural methods to probe not only neuronal but also astrocyte status may be of particular relevance to PD. Ample evidence from other diffusion-weighted imaging studies demonstrates that diffusion microstructure imaging is sensitive to changes in astrocyte and glial density and conformation due to pathology (18–20). Using a combination of diffusion, T1-weighted, and T2-weighted imaging to produce comprehensive MRI metrics has been shown to strongly correlate with increased glial fibrillary acidic protein deposition, a marker of astrogliosis (18). In rodent models, standard apparent diffusion coefficient measurements of isotropic diffusion were significantly associated with astrocytic markers measured via fluorescence microscopy (21). Furthermore, diffusion microstructure measurements made using mean apparent propagator MRI have been shown to be significantly correlated with astrogliosis in *ex vivo* examinations of chronic traumatic encephalopathy (19). This validation of diffusion MRI markers of astrogliosis using rodent histology and *ex vivo* human histology suggests that similarly positioned microstructural models are sufficiently sensitive to interpret changes as astrocytic in origin, depending on the clinical context *in vivo*. Our preclinical work indicates that morphological changes in astrocytes may be associated with exercise and fitness and that activation of astrocytes may underlie the beneficial effects of exercise in PD (16, 17) Looking for specific regions of the brain that might be vulnerable to change early in PD symptomology, the cholinergic basal forebrain and the nucleus basalis of Meynert in area 4 (CH4) has been implicated in a number of studies as involved in the spread of PD and in specific PD symptomology (5–7).

This study utilizes several advanced diffusion microstructure metrics to characterize the effects of PD at the cellular and sub-cellular level. These metrics (together with conventional structural MR volumetry) were sampled bilaterally in nine subcortical structures: the amygdala and hippocampus; the caudate, putamen, and nucleus accumbens; the thalamus and globus pallidus; and Ch4 and Ch123. These structures vary in the degree to which they suffer from PD pathology and in their relationship to the central DAergic and cholinergic systems attacked by PD. Among these structures, the amygdala and hippocampus are major mesial temporal lobe (MTL) regions. Some amygdalar subnuclei already evince alpha-synuclein load at Braak Stage 4; the remaining subnuclei and the entire hippocampus are impacted by Stages 5–6 (3). Neither the amygdala nor the hippocampus is appreciably recipient of DAergic innervation from the substantia nigra pars compacta. The amygdala (alongside the neocortex) is innervated with ACh by Ch4 and the hippocampus by Ch123 (22, 23). The caudate and putamen, however, are indirectly but strongly impacted by PD, as they are the major sites of DA output from the compacta (24). The accumbens, in contrast, receives its DA input from the ventral tegmental area (VTA) (25). Striatal nuclei receive only minor ACh input from midbrain or forebrain centers, as their ACh innervation is primarily intrinsic, from cholinergic interneurons (26). While the globus pallidus is not a major site of synuclein accumulation in PD (27, 28), its internal segment is highly relevant to the motor symptoms of PD and their treatment, as it is a node in both the direct and indirect pathways (29). The globus pallidus probably receives its ACh input from the pedunculopontine (Ch5) and the laterodorsal tegmental nuclei (Ch6) (26). The major cholinergic input to the thalamus is from Ch5–Ch6 (30); however, the nucleus basalis of Meynert (CH4) has been widely reported to supply efferent projections to the thalamus (31–33). Ch123 suffers synuclein deposition in Stage 3, Ch4 in Stages 3 and 4 (3, 34–37). As indicated, both serve as major sources of cholinergic output to the rest of the brain (38, 39). Using diffusion

10.3389/fneur.2026.1863964

TABLE 1 Patient demographics and motor and cognitive symptoms of PD at baseline and 18-month follow-up.

Measure	Units	Baseline	Follow-up	*p*-longitudinal
Demographics				
Sex	#m/#fm	10/12	--	--
Age	years	63.8 ± 9.7	--	--
Formal Education	years	17.27 ± 1.6	--	--
Time Since First Diagnosis	years	3.7 ± 2.6	--	--
Levadopa Equivalent Daily Dose	mg	474.3 ± 317.78	--	--
Motor symptoms				
MDS-UPDRS	Total Score	20.89 ± 9.71	15.50 ± 20.11	0.1538
Cognitive symptoms				
MOCA	Total Score	26.57 ± 2.27	26.30 ± 2.52	0.6799
Executive Function	Z-Score	0.174 ± 1.01	−0.085 ± 1.37	0.4088
Attention	Z-Score	−0.00075 ± 0.988	−0.188 ± 1.27	0.5262
Language	Z-Score	0.227 ± 1.00	0.1633 ± 1.02	0.807
Memory and Visuospatial	Z-Score	0.201 ± 0.772	0.025 ± 0.930	0.4285
Motor performance				
Latent Fitness	Total Score	0.235 ± 0.368	0.352 ± 0.423	0.4249

Also listed are baseline and follow-up latent fitness scores. Physical exercise is a well-known, recently proposed therapy for PD. Although patients were neither encouraged nor discouraged to exercise as part of the study, many PD patients will adopt increased exercise on their own. Thus, this fitness metric was assayed to assess potential effects of fitness on study outcomes. Data are the number of patients and/or mean ± standard deviation across the entire sample of $N = 22$. *p*-values are for linear mixed model F-tests comparing follow-up to baseline scores, controlling for age, sex, years after PD diagnosis, total brain volume, days between the baseline and follow-up visit, and scanning site. Medication was not reported to have changed between baseline and follow-up. MDS-UPDRS = Movement Disorders Society-Unified Parkinson's Disease Rating Scale Motor Score Part III, a standard clinical test of motor symptoms of PD; high scores are "bad." MOCA = Montréal Cognitive Assessment, a test of global cognition commonly used as a clinical screener for dementia; high scores are "good." Z-scores were computed as composites of multiple tests in each of four cognitive domains (see text); high Z-scores are "good." Latent fitness is an in-house-developed measure of physical fitness, with higher scores representing superior performance. A similar table for demographic, behavioral, and control metrics collected as part of this study, stratified by collection site, is available in Supplementary Table 1.

tractography, we additionally evaluated the structural connectivity between each structure (caudate, amygdala, thalamus, and nucleus accumbens) and Ch4.

The microstructural metrics were acquired longitudinally in a cohort of PD patients with well-characterized motor and cognitive symptoms. We assessed the relationships between each regional MR metric and symptom change between baseline and follow-up. Although exercise was not a planned intervention in this sample, a "latent fitness" measure was acquired at baseline and at the 18-month follow-up for each patient. This permitted us to assess the effects of fitness on MR endpoints.

Methods

Participants

Subjects diagnosed with PD were recruited from a cohort that was participating in an observational study examining associations between motor skill fitness and cognitive function over a 2-year period. Between 2018 and 2020, participants were recruited through movement disorder clinics at the Department of Neurology at the University of Southern California and the Veterans Affairs San Diego Healthcare System/University of California, San Diego, and through surrounding community groups. Written informed consent was obtained from all participants, and all study procedures were approved and affirmed by the Institutional Review Boards (IRBs) at each respective institution. After performing quality control on the imaging data and excluding any subject with missing data, 22 subjects (12 female) were used in the final analysis. Subject mean age at baseline was 63.83 years ± 9.70 SD (male 69.29 years ±7.93 SD; female 60.36 years ±6.37 SD). Subjects had been diagnosed with PD on average 3.72 years ±2.65 SD (male 3.14 years ±1.74 SD, female 4.09 years ±3.04 SD) before the study baseline. Subjects returned for follow-up evaluation at 18 months. All imaging and clinical assessments were obtained at baseline and at 18-month follow-up. All subjects were Hoehn & Yahr Stage 2, with the exception of a single individual who was stage 1; stages did not change across the study period. All measurements were obtained in the 'ON' medication state. Informed consent was obtained from all participants, and all study procedures were approved by the appropriate Institutional Review Board (IRB). A summary of all participants' metrics in cognitive and fitness tests is reported in Table 1.

Measures of cognitive performance

The Montreal Cognitive Assessment (MOCA) (40) was administered by two MoCA-certified, clinical neuropsychologists (A. J. P. and D. M. S., respectively) as a screening of general cognitive ability[1]. The MOCA is a screening measure of cognitive impairment

1 The Montreal Cognitive Assessment (MoCA) currently requires healthcare professionals to complete mandatory training and certification to administer and score the paper version, with certification enforcement effective from September 2019 and full access blocked by September 2020 if not certified. Interpretation of the MoCA must be conducted by trained professionals with clinical expertise. The MoCA assessments administered in this study were acquired under USC Study ID: HS-18-00323 (Giselle Petzinger, M.D., P.I.) during the period of 5/10/2019 to 9/27/2019 - prior to the period of mandatory MoCA approval. Authors A.J.P. (USC) and D.M.S. (UCSD) are both licensed by the State of California as clinical neuropsychologists who, in their role as professional clinicians on our study team, collected these assessment data. They both hold

in people with PD recommended by the MDS (41). Participants completed tests of attention, working memory, language, visuospatial function, executive function, and episodic memory (42). Attention was measured by (i) the number of seconds to complete the color naming subtest from the Delis Kaplan Executive Function System (D-KEFS) Color Word Interference Test (CWIT) (43), (ii) the number of seconds to complete the word reading subtest from the CWIT, and (iii) the total score for the forward digit span condition of the Adaptive Digit Ordering Test (DOT-A) (44). The total raw score from the digit sequencing condition of the DOT-A was used to measure working memory. The confrontational naming aspect of language ability was measured by the total number of correct responses provided spontaneously or with semantic cueing on the Boston Naming Test (45). The verbal fluency aspect of language was measured by the total correct number of words on the D-KEFS Letter Fluency test (phonemic fluency), while the D-KEFS Category Fluency test measured semantic fluency. Verbal episodic memory was measured by the total number of correct words recalled across the five immediate recall trials (IR) of the 2nd Edition of the California Verbal Learning Test (CVLT-II) (46) and the total number of words recalled on the long-delayed free recall condition of the CVLT-II (CVLT-II LD). Non-verbal episodic memory was measured by immediate and delayed recall from the Brief Visuospatial Memory Test-Revised (47). Visuospatial ability was measured by the total raw score on the Judgment of Line Orientation Test (48) and the total raw score on the Hooper Visual Organization Test (49). Executive function was measured using the number of perseverative responses on the Wisconsin Card Sorting Test-64 (50), the number of seconds to complete the color-word inhibition subtest of the D-KEFS CWIT, the number of seconds to complete the inhibition/switching subtest from the D-KEFS CWIT, and the number of correct words produced on the verbal fluency switching subtest from the D-KEFS verbal fluency test. These cognitive evaluations were then z-scored and collated into a single metric for each individual cognitive domain, including attention, working memory, language, visuospatial function, executive function, and episodic memory.

Participants self-reported their age, years of formal education, sex, and number of years since diagnosis. The Montreal Cognitive Assessment (MOCA) (40) was administered as a screening of general cognitive ability. The MOCA is a screening measure of cognitive impairment in people with PD recommended by the MDS (41). Motor symptom severity was assessed using the Movement Disorders Society-Unified Parkinson's Disease Rating Scale (MDS-UPDRS) motor score part III (51).

Measurement of motor performance

In recent years, potential beneficial effects of physical exercise on PD, especially its cognitive symptoms, have been investigated intensively (52), including by our laboratory (16, 17). The effects of exercise on PD were not part of the original specific aims of this study, and patients were neither encouraged nor discouraged from changing their exercise habits between baseline and follow-up. Knowledge of the benefits of exercise, both generally and specifically for PD, is, however, widespread in clinical populations, and many PD patients are prone to increase their level of physical exercise on their own, even without a physician's recommendation. We felt it would be remiss not to take this factor into account. Therefore, as an adaptive strategy, each patient underwent an assessment of physical fitness, yielding a Latent Fitness Score at baseline and follow-up. Motor skill fitness was assessed using objective and standardized clinical measures that include upper limb fine and coarse motor functions, balance, coordination, agility, and endurance, and that require timed performance in most items. Objective assessments included the following: (1) the Physical Performance Test (PPT) (53), (2) the Short Physical Performance Battery (SPPB) (54), (3) the Timed Up and Go (TUG) test (55), and (4) the Ten-step Test (TST) (56). For this study, a latent factor analysis approach was used to estimate motor skill fitness at baseline and follow-up for each study participant. The advantages of the latent factor approach are as follows: (i) it captures the variance shared among multiple individual tests within a construct (e.g., motor skill fitness) and ultimately minimizing measurement error; (ii) it reduces the number of statistical tests; and (iii) it provides a means to aggregate data that represent a similar theme or construct. First to determine the latent factor for motor skill fitness, raw scores for all motor skill assessments, including the PPT, SPPB, TUG and TST, were transformed so that for all tests higher scores represented better performance. Standardized z-score for each test was then calculated based on the mean and standard deviation. Next, a latent factor for motor skill fitness was generated using a structural equation modeling (SEM) that loaded all four clinical assessments. The SEM estimating the motor skill fitness latent factor had strong model fit (Chi-square = 0.021 (2), $p = 0.90$; Confirmatory Fit Index = 1.00; Root Mean Square Error of Approximation = <0.001). The factor and standardized loadings between the four individual component tests and the final latent fitness metric have been previously published as Supplementary Figure 1 (57).

Image acquisition

Diffusion, T1-weighted, and T2-weighted images were acquired from each subject at baseline and follow-up. Diffusion images were acquired with an isotropic voxel size of $1.7\times1.7\times1.7mm^3$, 120 non-colinear gradient directions at b = 3,000 s/mm^2, 30 at b = 1,300 s/mm^2, 30 at b = 300 s/mm^2, 12 at b = 80 s/mm^2, and 12 at b = 0. T1-weighted MPRAGE images were collected with a FOV of 208x300x320, and an isotropic voxel size of $0.8\times0.8\times0.8mm^3$. Images were acquired on a Siemens 3 T Prisma system at USC and on a GE Healthcare 3 T MR 750 system at the San Diego VA. Acquisition was identical at each site, with the exception of the MPRAGE having a TR/TE = 2400/2.22 ms at USC and TR/TE = 2852/3.548 ms at San Diego. The recruitment site was included as a factor in all imaging analyses.

Structural MRI post-processing

All images were analyzed in line with previously published research (58–60). In brief, T1w images were analyzed using the *recon-all* pipeline in FreeSurfer for volumetric components (61). FreeSurfer automatically generated gray matter masks (regions-of-interest—ROIs) for multiple subcortical structures taken from the Destrieux cortical atlas (62) bilaterally and calculated the volume of each. All microstructural metrics below were averaged within these ROIs. MR endpoints were averaged across the left and right of each ROI. ROIs included the amygdala, hippocampus, caudate, putamen, nucleus accumbens, globus pallidus, and thalamus.

current formal permissions to administer the MoCA assessment.

Diffusion MRI post-processing

Diffusion images were denoised (63), corrected for Gibbs ringing artifacts (64), and corrected for inhomogeneity fields using FMRIB software library (FSL) *topup* and *eddy* commands utilizing outlier detection and replacement (65–67). The final preprocessed diffusion images were up-sampled to an isotropic voxel size of $1.3\times1.3\times1.3mm^3$ (68), and only the b = 3,000 s/mm^2 images were used as an outer b-value shell. White matter (WM), gray matter (GM), and cerebrospinal fluid (CSF) tissue response functions were generated using the Dhollander algorithm (69), and single-shell 3-tissue-constrained spherical deconvolution were used to generate the WM fiber orientation distribution (FODs) and GM and CSF representations. Three-Tissue Constrained Spherical Deconvolution (70–73) was used to calculate the voxel-wise maps of the fraction of signal arising from each of three compartments: an intracellular anisotropic (ICA), intracellular isotropic (ICI), and extracellular isotropic freely diffusing water (ECI) compartment by setting the sum of all FOD coefficients equal to unity. WM-FODs were then used to create a cohort-specific template with a subset of all individuals in the cohort (74). All subject's WM-FODs were registered to this template using an affine nonlinear transform warp with reorientation of the FODs, and then the template was registered to a b-value-matched template in stereotaxic montreal neurological institute (MNI) space (75, 76). A fixel-based morphometry (FBM) (74, 77) approach was used to estimate the intra-axonal cross-sectional area within each voxel to be used as an apparent axonal volume fraction (AVF). A T2w image was obtained by extracting and averaging the b = 0 image from the preprocessed diffusion images. T1w and T2w images were processed as described in the MICA-MNI pipeline (78), including N4-bias correction (79), rescaling both images from 0 to 100, co-registration using a rigid transform (79), and subsequently registration to the cohort-specific template using the same warp as the diffusion images. The aggregate g-ratio was calculated on a voxel-wise basis according to Stikov et al. and was used according to Mohammadi and Callaghan, identically to the calculation in Newman et al. (59, 80–83). As a measure of intra-axonal volume, the fiber density cross section was used as the AVF (74). As a metric of myelin density, the T1w/T2w ratio was used as the myelin volume fraction (MVF). Aggregate conduction velocity was calculated based on the calculations of Rushton (84) and Berman et al. (85), again, identically to the calculation in Newman et al. (59). Each of these six different voxel-wise microstructure metrics is displayed in Figure 1, and was calculated for each voxel of the brain, from each subject, at both baseline and follow-up for this study.

Diffusion tractography

Whole-brain tractograms were generated for each subject at baseline and follow-up using Mrtrix3 (86). Diffusion image WM-FODs generated previously were used to derive the principal direction of diffusion in each brain voxel, and the output from FreeSurfer was used to generate a white matter–gray matter interface mask for seeding for an anatomically constrained tractography approach. Ten million tracts were generated using the iFOD2 probabilistic tracking algorithm, which was then reduced to 2 million based on the FOD lobe integral using the spherically informed filtering of tracts (SIFT) algorithm (86, 87). SIFT removes tracts in a systematic manner reliant on the underlying axonal anatomy to ensure remaining tracts are related to connectivity strength and allow for direct comparison between subjects. By normalizing the number of tracts consistent across individuals, this method allows direct numerical comparison of streamline counts for identical ROIs between individuals.

The goal of tractography was to quantify the diffusion-based structural connectivity between four of our subcortical ROIs and Ch4 (the location of which is displayed in Figure 2). A tract rendered by the algorithm as described above was counted as connecting Ch4 with the ROI and included in the count for statistical analysis if it crossed both Ch4 and the ROI in question. The "structural connectivity" of each Ch4-ROI pair was equal to the number of tracts in the count. The four ROIs (amygdala, caudate, putamen, and thalamus) were selected

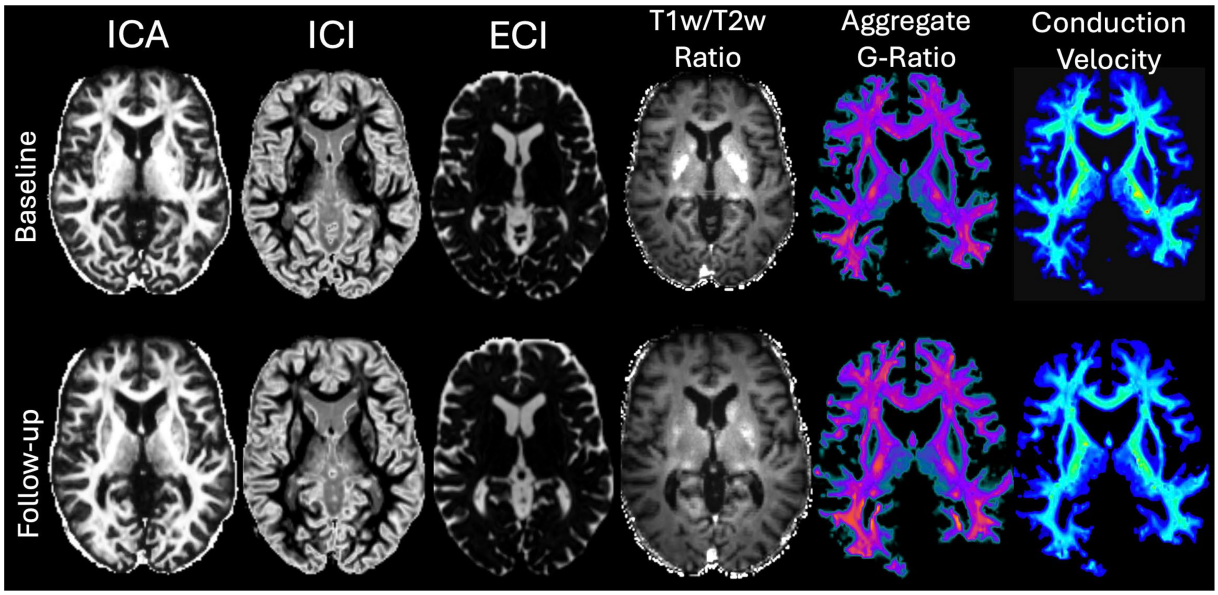

FIGURE 1
Representative native-space maps of each microstructural metric analyzed in this study from baseline and follow-up scans from a single subject. Each microstructural metric constitutes a single voxel-wise scalar value for mean aggregation within an ROI.

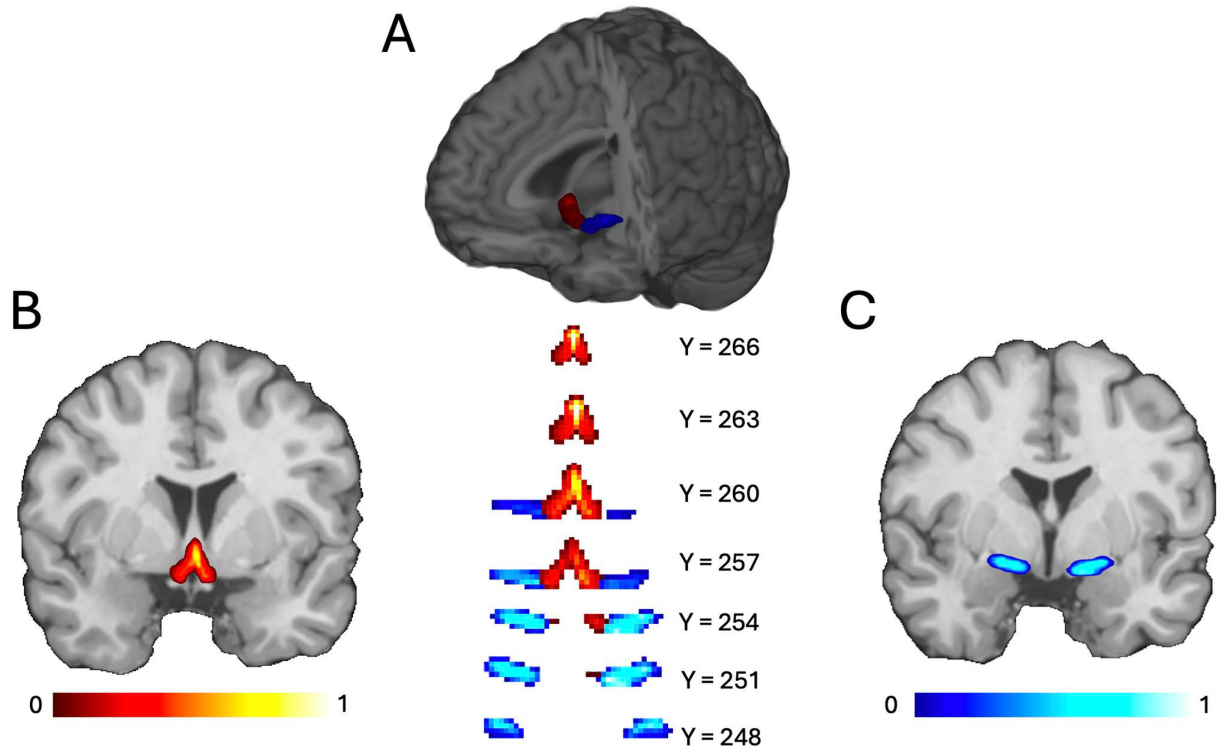

FIGURE 2
(A) Illustration of the placement of the Lorio et al. CH4 **(B)**, and **(C)** CH123 probabilistic masks. The masks were thresholded at 80% probability to reduce noise from anatomical or registration placement.

based on known Ch4 afferents from histological examination that overlapped with ROIs included in this study (31).

Statistical analysis

All analyses were made using the linear mixed effects (*lmer*) package in R using type III F tests. All models were controlled for using subject age, sex, years after PD diagnosis, total brain volume without ventricles calculated by FreeSurfer, days between the baseline and follow-up visit, and scanning site. These confounding variables were selected for their scientific merit and previously observed interactions with microstructural measurements (60, 88, 89).

The first analysis examined longitudinal changes from baseline to follow-up in motor symptoms, cognitive symptoms, and latent fitness. There was no correction for multiple comparisons for the first analysis. The second analysis examined the same in volume and the six microstructural metrics in the nine ROIs. The third analysis examined the effects of baseline values of volume and each of the six microstructural metrics in each ROI on longitudinal changes in motor symptoms, cognitive symptoms, and latent fitness. Effects on latent fitness were also assessed using both baseline and follow-up latent fitness scores separately. The fourth analysis examined longitudinal changes in structural connectivity for each of the four Ch4-ROI connectivity pairs. The fifth analysis examined the effects of baseline values of structural connectivity for each of the four Ch4-ROI pairs on longitudinal changes in motor symptoms, cognitive symptoms, and latent fitness, and separately on baseline and follow-up fitness. For the second and subsequent analyses, multiple comparisons were corrected for using the false discovery rate (FDR) under the Benjamini–Hochberg procedure.

Results

Imaging metrics

Summary values for each microstructural metric in each ROI are shown in Figure 3. These values and standard deviations are numerically presented for each timepoint in Supplementary Table 2. There was no significant difference in any microstructural metrics after Benjamini and Hochberg analysis between baseline and follow-up. The summary values for each of the volumetric subcortical ROIs available from FreeSurfer are presented in Figure 4. Controlling for total brain volume, there was a significant difference between baseline and follow-up in the hippocampus ($F = 16.65$, $p < 0.001$), pallidum ($F = 11.22$, $p < 0.001$), putamen ($F = 57.61$, $p < 0.001$), caudate ($F = 129.25$, $p < 0.001$), and thalamus ($F = 13.21$, $p < 0.001$). There was no significant difference between baseline and follow-up volumes of the accumbens ($F = 1.56$, $p = 0.211$ n.s.). When the analysis was redone using intracranial volume instead of total brain volume as a control, there was a significant difference between baseline and follow-up in the volume of the accumbens ($F = 6.76$, $p < 0.01$), hippocampus ($F = 13.84$, $p < 0.001$), pallidum ($F = 62.12$, $p < 0.001$), putamen ($F = 336.23$, $p < 0.001$), caudate ($F = 83.19$, $p < 0.001$), and thalamus ($F = 5.46$, $p < 0.05$). Interestingly, there was no significant relationship between longitudinal timepoint and total brain volume in models considering the putamen, hippocampus, or pallidum, suggesting that these areas may change at similar rates to the brain as a whole. In the caudate and thalamus, both longitudinal timepoint and total brain volume were highly significant, suggesting that these areas may be relatively increasing in volume compared to the brain as a whole

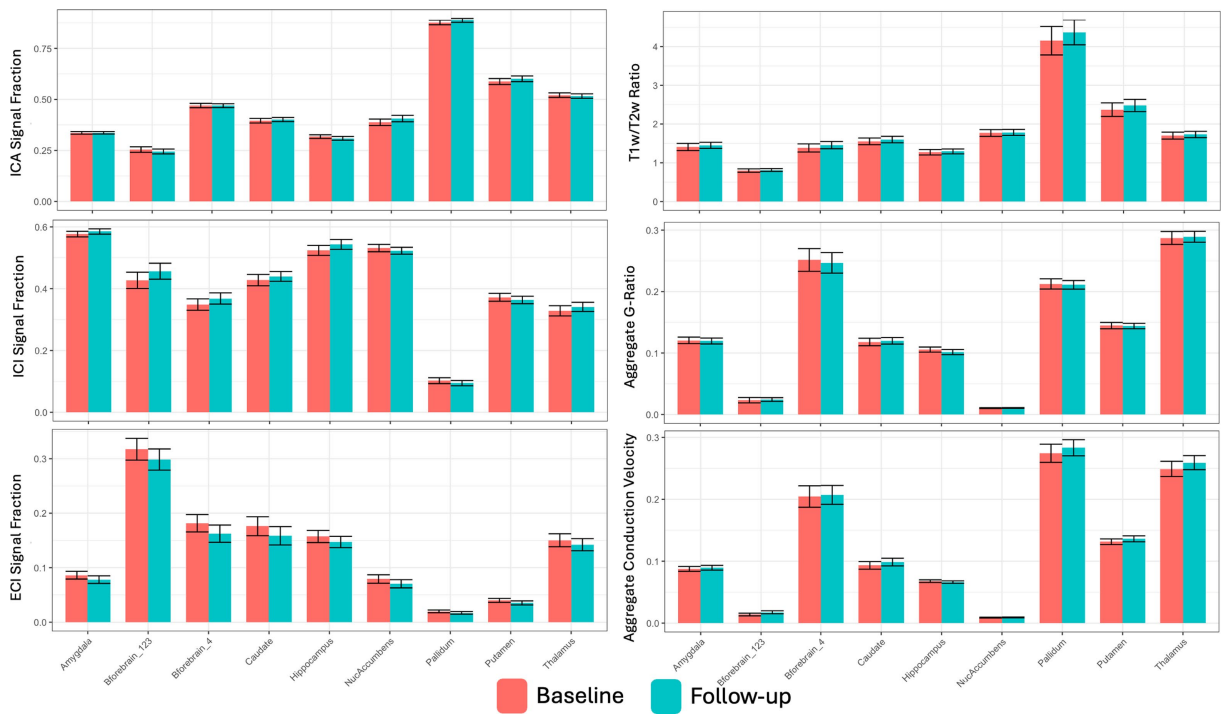

FIGURE 3
Charts displaying baseline and follow-up means and standard deviations for each microstructural metric in each ROI examined. Despite the focus on similar subcortical gray matter structures, there was a wide degree of variation in absolute microstructural values across the ROIs examined. No change from baseline to follow-up was significant after multiple comparison correction. All values displayed in these charts are listed in Supplementary Table 1. ECI, extracellular isotropic; ICI, intracellular isotropic; ICA, intracellular anisotropic.

(Figure 4). In all brain areas, intracranial volume was significantly associated with changes in regional volume.

Associations of MR metrics with longitudinal changes in motor symptoms, cognitive symptoms, and latent fitness

Main effects of volumes and microstructural metrics in each of the nine subcortical ROIs on motor symptoms, cognitive symptoms, and fitness can be found in Supplementary Tables 3–8 (3: MOCA, 4: executive function Z-score, 5: attention Z-score, 6: language Z-score, 7: memory–visuospatial Z-score, 8: latent fitness controlled for baseline fitness). Table 2 lists statistical results and β coefficients for regional associations between baseline MR metrics and longitudinal changes in symptom and fitness scores that remained significant after FDR correction. In the caudate, changes in executive function, attention, and memory and visuospatial Z-scores (all $p < 0.05$) varied significantly with ICI. ICI had a sparingly significant relationship with change in the language Z-score ($p = 0.053$). The volume of the caudate was also significantly associated with change in the attention Z-score ($F_1 = 10.06$, $p < 0.01$). In the putamen, changes in executive function and memory–visuospatial Z-scores varied with ICI (both $p < 0.05$). In the nucleus accumbens, changes in executive function and memory–visuospatial Z-scores varied significantly with ICI (both $p < 0.05$), and change in the language Z-score varied sparingly significantly with ICI ($p = 0.053$). ICI of the thalamus varied significantly with a change in the executive function Z-score ($p < 0.05$). In Ch4, ICI varied with changes in latent fitness ($p < 0.01$) and *ICA* varied with changes in MOCA ($p < 0.01$). Volumetric associations with motor symptoms, cognitive symptoms, and fitness can be found in Supplementary Table 9. The bilateral volume of the caudate was significantly associated with attention ($p < 0.01$). No other significant associations were found between MR metrics and symptom or fitness scores in any ROI examined.

Diffusion tractography

The number of tracts connecting the CH4 with known afferent subcortical structures was examined in longitudinal models identical to the previous tests (Figure 5). The connectivity between the CH4 and thalamus was significantly associated with baseline motor skill fitness ($F = 5.176$, $p < 0.05$). It was nearly significantly associated with follow-up fitness ($F = 4.33$, $p = 0.059$, n.s.) and with the MOCA ($F = 4.03$, $p = 0.066$, n.s.). This matched microstructure results for the CH4 generally. The connectivity between the CH4 and the caudate, putamen, and amygdala was not significant for any of the behavioral metrics tested in this study. The full list of all statistical tests and β coefficients between connectivity and behavioral metrics is available in Supplementary Table 10.

Discussion

This study examines a longitudinal cohort of PD patients using advanced diffusion microstructure analysis to evaluate several regions of the subcortical gray matter and basal ganglia for associations with clinically relevant cognitive measures and level of motor skill fitness. Associations were found between executive, attention, language, cognition, and latent fitness scores and intracellular isotropic signal across

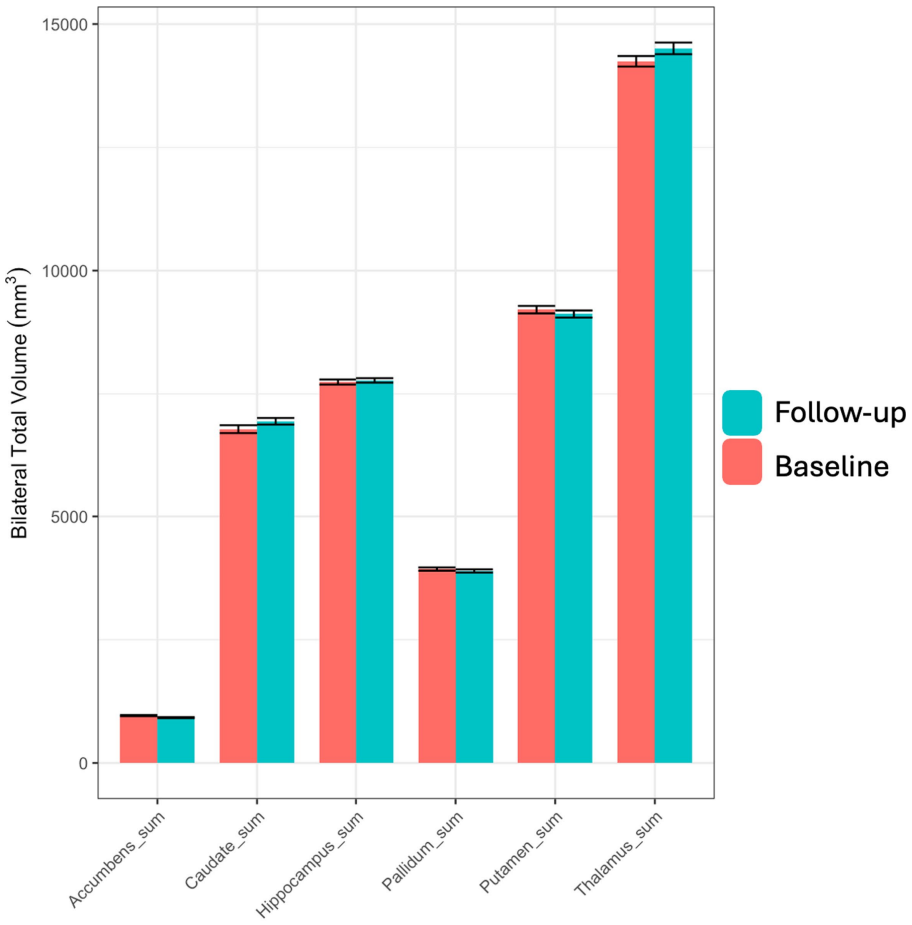

FIGURE 4
Charts displaying the baseline and follow-up volumes (group-means and standard deviations) for each ROI volumetric measurement available from the FreeSurfer recon-all analysis pipeline. There was a split in the direction of volumetric changes, with the thalamus, hippocampus, and caudate significantly increasing and the putamen and pallidum significantly decreasing between baseline and follow-up (all $p < 0.05$ following FDR). There was a non-significant decrease in the volume of the accumbens between baseline and follow-up.

TABLE 2 Associations of regional MR metrics at baseline with longitudinal changes in motor and cognitive scores and fitness.

ROI	MOCA	Executive function	Attention	Language	Memory and visuospatial	Latent fitness
Amygdala	NA	NA	NA	NA	NA	NA
Cholinergic Basal Forebrain Area 1,2,3	NA	NA	NA	NA	NA	NA
Cholinergic Basal Forebrain Area 4	ICA $p < 0.01$	NA	NA	NA	NA	ICI $p < 0.01$
Caudate	NA	ICI $p < 0.05$	ICI $p < 0.05$	ICI $p = 0.053$	ICI $p < 0.05$	NA
Hippocampus	NA	NA	NA	NA	NA	NA
Nucleus Accumbens	NA	ICI $p < 0.05$	NA	ICI $p = 0.053$	ICI $p < 0.05$	NA
Pallidum	NA	NA	NA	NA	NA	NA
Putamen	NA	ICI $p < 0.05$	NA	NA	ICI $p < 0.05$	NA
Thalamus	NA	ICI $p < 0.05$	NA	NA	NA	NA

For each ROI-symptom domain combination, MR metrics are listed that showed a significant relationship with the symptom or fitness score (p-values for linear mixed model, FDR-corrected). Ns: No significant findings. The ICI metric (reflecting mainly diffusion within neuronal and astrocytic perikarya) in three striatal nuclei (caudate, putamen, and accumbens) and the thalamus predicted change in multiple cognitive domains. Caudate volume additionally predicted change in attention. In Ch4, ICA (reflecting mainly diffusion within axons and neurites) predicted change in global cognition (MOCA), and ICI predicted change in fitness. No other volume or microstructure-symptom associations were significant after multiple comparison correction. Main effects of volumes and microstructural metrics in each of the nine subcortical ROIs on motor symptoms, cognitive symptoms, and fitness can be found in Supplementary Tables 3–8 (3: MOCA, 4: Executive function Z-score, 5: Attention Z-score, 6: Language Z-score, 7: Memory–visuospatial Z-score, 8: Latent fitness controlled for baseline fitness).

10.3389/fneur.2026.1863964

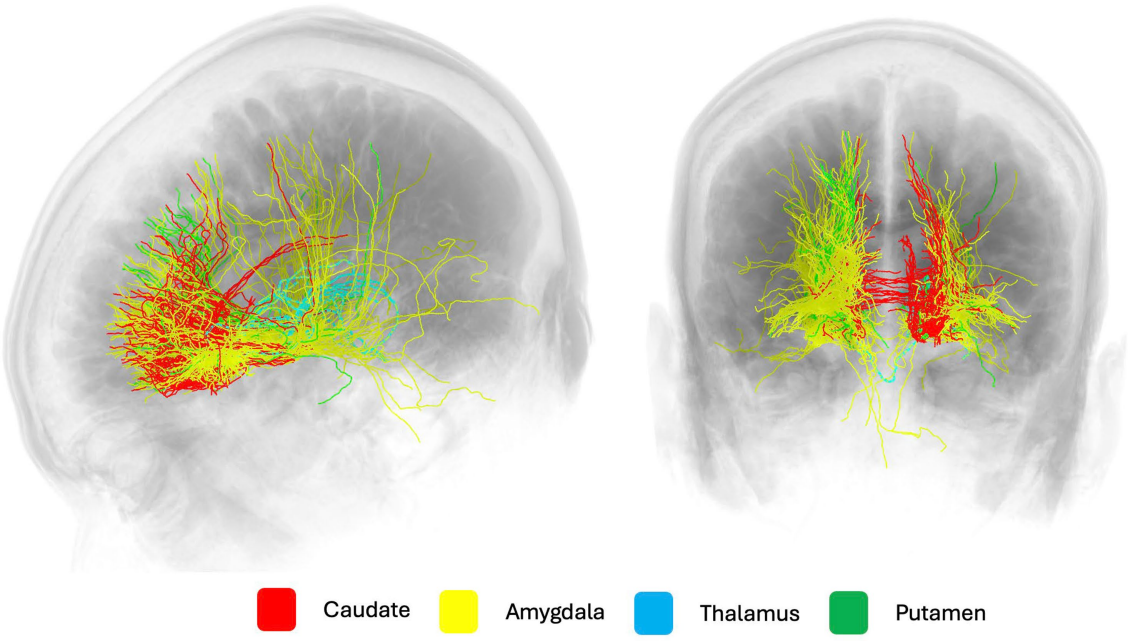

FIGURE 5
Example from a single subject showing connections between CH4 and the caudate, amygdala, thalamus, and putamen. All regional masks were applied bilaterally throughout the cohort. Tracts that crossed through both CH4 and the relevant ROI were counted to capture all available connections from the probabilistic tracking method.

five subcortical and basal ganglia ROIs (caudate, putamen, thalamus, nucleus accumbens, and CH4). Executive function and the cognitive composite score were significantly correlated with the intracellular isotropic signal across all these regions, excluding the basal forebrain area, CH4. Intracellular anisotropic signal was related to the MOCA score in CH4. Volumetrically, there was a significant change between subject baseline and follow-up in five ROIs; however, none of these changes was correlated with measures of cognitive function or motor skill fitness. Structural connectivity between the CH4 and the thalamus was found to be significantly associated with motor skill fitness. Taken together, these findings suggest that the ICI metric in the striatum and thalamus fairly prognosticates evolution in specific cognitive domains in PD. Global cognitive status and exercise-mediated recovery of cognitive function may be affected by axonal projections, including the thalamus.

Although six separate microstructure metrics were assayed, nearly all significant associations with cognitive symptoms and fitness involved a single metric, the ICI. Crucially, as the signal fractions (ICI, ICA, and ECI) are summed to unity, the changes observed in this study are relative to the signal from each of the other compartments and are not necessarily indicative of change in the overall signal. Observing the longitudinal changes over time in this cohort, the increase in intracellular isotropic signal appears to occur with a decrease in extracellular free water, with the intracellular anisotropic signal unchanged. The increase in extracellular free water is typically thought to arise from cellular atrophy and degeneration, as cellular bodies are lost, the resulting extracellular space is filled with freely diffusing fluid (11, 90–92). An increase in intracellular isotropic signal, however, is thought to involve increased neuronal cell somas or glial structures. A key component of the 3 T-CSD microstructural model structure is the ability of each compartment to not only be detected but also to have signal associated with other compartments identified and removed through the repeated single-shell constrained spherical deconvolution framework. The intracellular isotropic compartment is thus positioned to interrogate non-axonal signal changes within even predominantly axonal areas and along tracts.

It has previously been noted that model-free diffusion microstructure models are specifically sensitive to astrogliosis and astrocyte reactivity (18, 19). Additionally, the isotropic diffusion model used in this study has previously been implicated in events known to be heavily affected by changes in glial cell density and conformation, such as pubertal development in adolescents (60). In both the intracellular signal fraction change observed in this study and the increase observed in puberty, it is proposed that conformational changes in glial cells underlie the observed microstructural change. Pubertal development is characterized by increased myelination throughout the cortex, performed by oligodendrocytes, and it is likely that the observed intracellular isotropic signal increases reflect oligodendrocyte proliferation and growth. In the current study, at the opposite end of the lifespan, the pathology of PD may potentially be inducing a reaction from various glial cells. Prior work in rodent models suggests that astrocyte activation and conformational change occur during PD (17). This has been suggested to be affected through exercise in PD, and in this study, we observe increased intracellular isotropic signal associated with motor skill fitness. This was observed to especially be the case in the CH4, a critical region associated with PD progression and symptomology (5–7). Although diffusion microstructure analysis is unable to positively identify a direct biological source for observed changes, given the contextual implication of astrocytes in animal models of PD, this finding is consistent with astrocytes being similarly implicated in the mediation of exercise-related effects in humans.

Consistent with a glial origin of our present findings is the lack of significant symptom associations with or longitudinal changes in the four microstructural metrics linked to axonal structure and function. T1w/T2w ratio measures myelin integrity, and ICA, aggregate g-ratio, and aggregate conduction velocity all characterize axonal properties.

While the ROIs examined in this study were predominantly gray matter structures, such as subcortical nuclei and cortex generally, they are still typically innervated by or act as the source of axons and thus may exhibit axonal effects on microstructural indices (59). The effect observed in this report for Ch4-thalamus structural connectivity may reflect an influence of axonal properties in the intervening white matter on attention and fitness in PD. A recent study using deep brain stimulation identified that connectivity between the pallidus and thalamus was correlated with worsening axial gain symptoms, whereas cerebellar lobes I–IV connectivity to thalamus predicted improvement at 36-month follow-up (93). The convergence of this interventional deep brain stimulation (DBS)-connectomic study with the CH4-thalamus connectivity and thalamic microstructural findings in this study independently identifies the thalamus as a critical connectivity node for motor performance in PD. Together, these supply an emerging body of evidence that connectivity between the CH4 and thalamus is a meaningful substrate for motor fitness.

Interestingly, several subcortical structures exhibited longitudinal volume changes in the absence of microstructural effects between baseline and follow-up. The caudate and thalamus were observed to significantly increase in volume between baseline and follow-up, in contrast to expected atrophy and volumetric decline. This may be due to measurement error in a small sample, but it is also possible that neuroinflammatory or compensatory processes over the short 18-month period played a larger role than long-term volume decline. Furthermore, these two areas are surrounded by WM and are relatively medial in the structure of the cortex. Extensive WM volume was not examined, and volume loss throughout the skeleton may have resulted in slightly larger estimates of regional gray matter. These volumetric changes were significant both relative to total brain volume and to estimated total intracranial volume. This suggests that changes in subcortical structures are not only occurring more rapidly than total cortical atrophy but are also scaled compared to total intracranial volume (which is more invariant across timepoints). Although microstructural changes have previously been shown to predate volumetric changes, the primary tissue compartment involved in these changes has typically been the extracellular free water compartment (91). Free water in the substantia nigra has also featured large in previous microstructure work in PD and has been proposed as a measure of the functional status of surviving dopaminergic nerve terminals (11). It is possible that the timespan between baseline and follow-up was too short for such effects to manifest, as no microstructural changes were significant between baseline and follow-up in the current study. The lack of free water (ECI) results also suggests that observed volumetric changes were not associated with atrophy or typical decline, but rather were in line with neuroinflammatory processes. The overall small number of participants who were able to complete the extensive battery of all imaging, cognitive, and fitness metrics may have contributed to less-than-expected longitudinal results.

Prior work tying altered fractional anisotropy to PD symptomology of various kinds supports the notion of altered microstructural properties in the brain in PD. A recent meta-analysis found that increased mean diffusivity was particularly sensitive to clinical PD parameters, similar to the ICI findings of our study (94). Compared to mean diffusivity, ICI is more specific than mean diffusivity to isotropic signal within cellular bodies. Mean diffusivity additionally includes the presence of the extracellular isotropic compartment. Thus, increased mean diffusivity may result from either increased cellularity or increased free water. The results of this study suggest that increased ICI is due to cellular change and not increased extracellular water. Some studies report an unexpected increase in fractional anisotropy in specific white matter tracts in PD. The positive associations observed in this study between Ch4-thalamus structural connectivity and attention and between Ch4 ICA and MOCA score are consistent with such findings.

This exploratory study remains limited by the small sample size spread across two different acquisition sites. The approach used in this study aimed to emphasize 'deep' over 'wide' data collection, with detailed latent fitness models examining motor control at a fine-grained level beyond typical approaches. Differences in data between sites were minimal (Table S1), and all analyses featured acquisition site as a control term; however, future studies would greatly benefit from higher numbers of participants. Future multi-site studies with more participants could integrate more sophisticated methods of site control, such as the ComBat algorithm (95). These findings should be validated in larger, independent longitudinal cohorts before their clinical applicability can be established. In addition, the lack of a healthy control group limits the conclusions that can be drawn from this study, as it is difficult to disassociate them from the typical aging process without adequate comparison. However, it should be noted that increased intracellular signal in early-stage PD has been identified by large consortium studies such as ENIGMA (96), which would support the ICI and volumetric results observed in this study. We would like to emphasize the importance of the highly detailed and thorough behavioral metrics, particularly the latent fitness metric, as key to associating changes in brain structure with physical activity even in a small clinical population. Using these methods in a larger cohort and with adequate healthy controls as a comparison group would enable greater inferences to be made about PD-related changes in the brain that drive PD manifestations.

This study utilizes a number of advanced diffusion microstructure metrics to evaluate a longitudinal cohort of PD patients. By finding widespread associations between an isotropic intracellular signal and cognitive and fitness metrics, this study suggests that increased cellularity, potentially from astrocytic glial cells, may support reduced symptoms of decline during PD and increased motor skill fitness. These results demonstrate the sensitivity of advanced diffusion cellular microstructure metrics to short-term changes in the brain in a clinical population and suggest that these metrics may be promising future biomarkers that can contribute to patient stratification or longitudinal disease monitoring, especially relating physical performance to neuronal changes.

Data availability statement

The raw data supporting the conclusions of this article will be made available by the authors, without undue reservation.

Ethics statement

The studies involving humans were approved by the Institutional Review Boards of the University of California San Diego and the

University of Southern California (Study ID: HS-18-00323). The studies were conducted in accordance with the local legislation and institutional requirements. The participants provided their written informed consent to participate in this study.

Author contributions

BN: Writing – review & editing, Investigation, Resources, Formal analysis, Data curation, Visualization, Writing – original draft. RF: Investigation, Writing – review & editing, Resources, Writing – original draft, Data curation, Formal analysis. ED: Investigation, Formal analysis, Resources, Data curation, Writing – original draft, Writing – review & editing. MJ: Project administration, Resources, Data curation, Writing – original draft, Methodology, Investigation, Conceptualization, Funding acquisition, Writing – review & editing, Supervision. AP: Supervision, Methodology, Data curation, Investigation, Writing – original draft, Resources, Conceptualization, Formal analysis, Writing – review & editing, Project administration, Funding acquisition. DH: Project administration, Writing – review & editing, Formal analysis, Writing – original draft, Methodology, Supervision, Investigation, Resources, Conceptualization. JO'N: Investigation, Conceptualization, Funding acquisition, Resources, Project administration, Supervision, Formal analysis, Writing – review & editing, Methodology, Writing – original draft. DS: Project administration, Formal analysis, Data curation, Methodology, Funding acquisition, Writing – review & editing, Investigation, Conceptualization, Writing – original draft, Supervision, Resources. GP: Formal analysis, Writing – original draft, Funding acquisition, Conceptualization, Resources, Supervision, Project administration, Data curation, Investigation, Writing – review & editing, Methodology. JV: Conceptualization, Writing – original draft, Methodology, Data curation, Investigation, Supervision, Resources, Formal analysis, Funding acquisition, Writing – review & editing, Project administration.

Funding

The author(s) declared that financial support was received for this work and/or its publication. This study was supported by grants from the US Department of Defense (U. S. Army, CDMRP), #W81XWH18-1-0666 (DH), #W81XWH19-1-0443 (MJ), #W81XWH18-1-0665 (GP), the Parkinson's Foundation (GP), and Kirk Hyde and Angie Proctor.

Conflict of interest

The author(s) declared that this work was conducted in the absence of any commercial or financial relationships that could be construed as a potential conflict of interest.

Generative AI statement

The author(s) declared that Generative AI was not used in the creation of this manuscript.

Any alternative text (alt text) provided alongside figures in this article has been generated by Frontiers with the support of artificial intelligence and reasonable efforts have been made to ensure accuracy, including review by the authors wherever possible. If you identify any issues, please contact us.

Publisher's note

All claims expressed in this article are solely those of the authors and do not necessarily represent those of their affiliated organizations, or those of the publisher, the editors and the reviewers. Any product that may be evaluated in this article, or claim that may be made by its manufacturer, is not guaranteed or endorsed by the publisher.

Supplementary material

The Supplementary material for this article can be found online at: https://www.frontiersin.org/articles/10.3389/fneur.2026.1863964/full#supplementary-material

References

1. Chaudhuri KR, Healy DG, Schapira AH. Non-motor symptoms of Parkinson's disease: diagnosis and management. *Lancet Neurol.* (2006) 5:235–45. doi: 10.1016/S1474-4422(06)70373-8

2. Sveinbjornsdottir S. The clinical symptoms of Parkinson's disease. *J Neurochem.* (2016) 139:318–24. doi: 10.1111/jnc.13691

3. Braak H, Del Tredici K, Rüb U, De Vos RA, Steur ENJ, Braak E. Staging of brain pathology related to sporadic Parkinson's disease. *Neurobiol Aging.* (2003) 24:197–211. doi: 10.1016/S0197-4580(02)00065-9

4. Lotharius J, Brundin P. Pathogenesis of Parkinson's disease: dopamine, vesicles and α-synuclein. *Nat Rev Neurosci.* (2002) 3:932–42.

5. Barrett MJ, Sperling SA, Blair JC, Freeman CS, Flanigan JL, Smolkin ME, et al. Lower volume, more impairment: reduced cholinergic basal forebrain grey matter density is associated with impaired cognition in Parkinson disease. *J Neurol Neurosurg Psychiatry.* (2019) 90:1251–6. doi: 10.1136/jnnp-2019-320450

6. Barrett MJ, Murphy JM, Zhang J, Blair JC, Flanigan JL, Nawaz H, et al. Olfaction, cholinergic basal forebrain degeneration, and cognition in early Parkinson disease. *Parkinsonism Relat Disord.* (2021) 90:27–32. doi: 10.1016/j.parkreldis.2021.07.024

7. Barrett MJ, Blair JC, Sperling SA, Smolkin ME, Druzgal TJ. Baseline symptoms and basal forebrain volume predict future psychosis in early Parkinson disease. *Neurology.* (2018) 90:e1618–26. doi: 10.1212/WNL.0000000000005421

8. Langley J, Huddleston DE, Chen X, Sedlacik J, Zachariah N, Hu X. A multicontrast approach for comprehensive imaging of substantia nigra. *NeuroImage.* (2015) 112:7–13. doi: 10.1016/j.neuroimage.2015.02.045

9. Le Berre A, Kamagata K, Otsuka Y. Convolutional neural network-based segmentation can help in assessing the substantia nigra in neuromelanin MRI. *Neuroradiology.* (2019) 61:1387–95. doi: 10.1007/s00234-019-02279-w

10. Dyrby TB, Innocenti GM, Bech M, Lundell H. Validation strategies for the interpretation of microstructure imaging using diffusion MRI. *NeuroImage*. (2018) 182:62–79. doi: 10.1016/j.neuroimage.2018.06.049

11. Ofori E, Pasternak O, Planetta PJ, Li H, Burciu RG, Snyder AF, et al. Longitudinal changes in free-water within the substantia nigra of Parkinson's disease. *Brain*. (2015) 138:2322–31. doi: 10.1093/brain/awv136

12. Lenka A, Ingalhalikar M, Shah A, Saini J, Arumugham SS, Hegde S, et al. Abnormalities in the white matter tracts in patients with Parkinson disease and psychosis. *Neurology*. (2020) 94:e1876–84. doi: 10.1212/WNL.0000000000009363

13. Theilmann RJ, Reed JD, Song DD, Huang MX, Lee RR, Litvan I, et al. White-matter changes correlate with cognitive functioning in Parkinson's disease. *Front Neurol*. (2013) 4:4. doi: 10.3389/fneur.2013.00037

14. Devignes Q, Viard R, Betrouni N, Carey G, Kuchcinski G, Defebvre L, et al. Posterior cortical cognitive deficits are associated with structural brain alterations in mild cognitive impairment in Parkinson's disease. *Front Aging Neurosci*. (2021) 13:13. doi: 10.3389/fnagi.2021.668559

15. Ofori E, Pasternak O, Planetta PJ, Burciu R, Snyder A, Febo M, et al. Increased free water in the substantia nigra of Parkinson's disease: a single-site and multi-site study. *Neurobiol Aging*. (2015) 36:1097–104. doi: 10.1016/j.neurobiolaging.2014.10.029

16. Lundquist AJ, Parizher J, Petzinger GM, Jakowec MW. Exercise induces region-specific remodeling of astrocyte morphology and reactive astrocyte gene expression patterns in male mice. *J Neurosci Res*. (2019) 97:1081–94. doi: 10.1002/jnr.24430

17. Petzinger GM, Walsh JP, Akopian G, Hogg E, Abernathy A, Arevalo P, et al. Effects of treadmill exercise on dopaminergic transmission in the 1-methyl-4-phenyl-1, 2, 3, 6-tetrahydropyridine-lesioned mouse model of basal ganglia injury. *J Neurosci*. (2007) 27:5291–300. doi: 10.1523/jneurosci.1069-07.2007

18. Benjamini D, Priemer DS, Perl DP, Brody DL, Basser PJ. Mapping astrogliosis in the individual human brain using multidimensional MRI. *Brain*. (2023) 146:1212–26. doi: 10.1093/brain/awac298

19. Gangolli M, Pajevic S, Kim JH, Hutchinson EB, Benjamini D, Basser PJ. Correspondence of mean apparent propagator MRI metrics with phosphorylated tau and astrogliosis in chronic traumatic encephalopathy. *Brain Commun*. (2023) 5:fcad253. doi: 10.1093/braincomms/fcad253

20. Sue YY, Stowe NA, Barnett BR, Dodd K, John-Paul JY. Microglial density alters measures of axonal integrity and structural connectivity. *Biol Psychiatry: Cognit Neurosci Neuroimaging*. (2020) 5:1061–8.

21. Li M, Liu Z, Wu Y, Zheng N, Liu X, Cai A, et al. In vivo imaging of astrocytes in the whole brain with engineered AAVs and diffusion-weighted magnetic resonance imaging. *Mol Psychiatry*. (2024) 29:545–52. doi: 10.1038/s41380-022-01580-0

22. Mesulam M, Johnson N, Krefft TA. Progranulin mutations in primary progressive aphasia: the PPA1 and PPA3 families. *Arch Neurol*. (2007) 64:43–7.

23. Mesulam M-M, Mufson EJ, Levey AI, Wainer BH. Cholinergic innervation of cortex by the basal forebrain: cytochemistry and cortical connections of the septal area, diagonal band nuclei, nucleus basalis (substantia innominata), and hypothalamus in the rhesus monkey. *J Comp Neurol*. (1983) 214:170–97.

24. Haber SN. The place of dopamine in the cortico-basal ganglia circuit. *Neuroscience*. (2014) 282:248–57. doi: 10.1016/j.neuroscience.2014.10.008

25. Chinta SJ, Andersen JK. Dopaminergic neurons. *Int J Biochem Cell Biol*. (2005) 37:942–6. doi: 10.1016/j.biocel.2004.09.009

26. Mesulam M-M, Hersh LB, Mash DC, Geula C. Differential cholinergic innervation within functional subdivisions of the human cerebral cortex: a choline acetyltransferase study. *J Comp Neurol*. (1992) 318:316–28.

27. Lavoie B, Smith Y, Parent A. Dopaminergic innervation of the basal ganglia in the squirrel monkey as revealed by tyrosine hydroxylase immunohistochemistry. *J Comp Neurol*. (1989) 289:36–52.

28. Parent A. Extrinsic connections of the basal ganglia. *Trends Neurosci*. (1990) 13:254–8.

29. Nambu A. A new dynamic model of the cortico-basal ganglia loop. *Prog Brain Res*. (2004) 143:461–6.

30. Pahapill PA, Lozano AM. The pedunculopontine nucleus and Parkinson's disease. *Brain*. (2000) 123:1767–83.

31. Gratwicke J, Kahan J, Zrinzo L, Hariz M, Limousin P, Foltynie T, et al. The nucleus basalis of Meynert: a new target for deep brain stimulation in dementia? *Neurosci Biobehav Rev*. (2013) 37:2676–88. doi: 10.1016/j.neubiorev.2013.09.003

32. Chen Z, Yang Y, Li M, Gao L, Qu WM, Huang ZL, et al. Whole-brain neural connectivity to cholinergic neurons in the nucleus basalis of Meynert. *J Neurochem*. (2023) 166:233–47. doi: 10.1111/jnc.15873

33. Levey AI, Hallanger AE, Wainer BH. Cholinergic nucleus basalis neurons may influence the cortex via the thalamus. *Neurosci Lett*. (1987) 74:7–13.

34. Meoni S, Macerollo A, Moro E. Sex differences in movement disorders. *Nat Rev Neurol*. (2020) 16:84–96. doi: 10.1038/s41582-019-0294-x

35. Candy J, Perry RH, Perry EK, Candy JM, Irving D, Blessed G, et al. Pathological changes in the nucleus of Meynert in Alzheimer's and Parkinson's diseases. *J Neurol Sci*. (1983) 59:277–89.

36. Gratwicke JP, Foltynie T. Early nucleus basalis of Meynert degeneration predicts cognitive decline in Parkinson's disease. *Brain*. (2018) 141:7–10. doi: 10.1093/brain/awx333

37. Liu L, Luo XG, Dy CL, Ren Y, Feng Y, Yu HM, et al. Characteristics of language impairment in Parkinson's disease and its influencing factors. *Transl Neurodegener*. (2015) 4:2. doi: 10.1186/2047-9158-4-2

38. Mesulam M. Cholinergic circuitry of the human nucleus basalis and its fate in Alzheimer's disease. *J Comp Neurol*. (2013) 521:4124–44. doi: 10.1002/cne.23415

39. Mesulam MM. The cholinergic innervation of the human cerebral cortex. *Prog Brain Res*. (2004) 145:67–78. doi: 10.1016/S0079-6123(03)45004-8

40. Nasreddine ZS, Phillips NA, Bédirian V, Charbonneau S, Whitehead V, Collin I, et al. The Montreal cognitive assessment, MoCA: a brief screening tool for mild cognitive impairment. *J Am Geriatr Soc*. (2005) 53:695–9. doi: 10.1111/j.1532-5415.2005.53221.x

41. Chou KL, Amick MM, Brandt J. *A recommended scale for cognitive screening in clinical trials of Parkinson's disease*, vol. 25Wiley Online Library (2010). p. 2501–7.

42. Litvan I, Goldman JG, Tröster AI, Schmand BA, Weintraub D, Petersen RC, et al. Diagnostic criteria for mild cognitive impairment in Parkinson's disease: Movement Disorder Society task force guidelines. *Mov Disord*. (2012) 27:349–56. doi: 10.1002/mds.24893

43. Delis D. C., Kaplan E., Kramer J. H. Delis-Kaplan executive function system assessment. *Assessment* (2001).

44. Werheid K, Hoppe C, Thöne A, Müller U, Müngersdorf M, von Cramon DY. The adaptive digit ordering test clinical application, reliability, and validity of a verbal working memory test. *Arch Clin Neuropsychol*. (2002) 17:547–65. doi: 10.1093/arclin/17.6.547

45. Kaplan E., Goodglass H., Weintraub S. Boston naming test the clinical neuropsychologist. Philadelphia: Lea & Febiger (2001).

46. Delis DC, Kramer JH, Kaplan E, Ober BA. California verbal learning test. *Assessment (N Y)*. (2000)

47. Benedict RH. *Brief Visuospatial Memory Test--Revised*. PAR (1997).

48. Benton AL, Varney NR, Hamsher K deS Judgment of line orientation. *APA PsycTests* (1983).

49. Boyd JL. A validity study of the Hooper visual organization test. *J Consult Clin Psychol*. (1981) 49:15–9.

50. Kong S, Thompson L, Iverson G, Heaton RK. *Wisconsin Card Sorting Test—64 Card Version Professional Manual*. Odessa, FL: Psychological Assessment Resources (2000).

51. Goetz CG, Tilley BC, Shaftman SR, Stebbins GT, Fahn S, Martinez-Martin P, et al. Movement Disorder Society-sponsored revision of the unified Parkinson's disease rating scale (MDS-UPDRS): scale presentation and clinimetric testing results. *Mov Disord*. (2008) 23:2129–70. doi: 10.1002/mds.22340

52. Ellis TD, Colón-Semenza C, DeAngelis TR, Thomas CA, Hilaire M-HS, Earhart GM, et al. Evidence for early and regular physical therapy and exercise in Parkinson's disease. *Semin Neurol*. (2021) 41:189–205. doi: 10.1055/s-0041-1725133

53. Reuben DB, Siu AL. An objective measure of physical function of elderly outpatients: the physical performance test. *J American Geriatrics Society*. (1990) 38:1105–12.

54. Guralnik JM, Simonsick EM, Ferrucci L, Glynn RJ, Berkman LF, Blazer DG, et al. A short physical performance battery assessing lower extremity function: association with self-reported disability and prediction of mortality and nursing home admission. *J Gerontol*. (1994) 49:M85–94.

55. Podsiadlo D, Richardson S. The timed "Up & Go": a test of basic functional mobility for frail elderly persons. *Journal of the American geriatrics Society,* (1991) 39:142–148.

56. Miyamoto K, Takebayashi H, Takimoto K, Miyamoto S, Morioka S, Yagi F. A new simple performance test focused on agility in elderly people: the ten step test. *Gerontology*. (2008) 54:365–72. doi: 10.1159/000146787

57. Petkus AJ, Foreman RP, Pilgrim M, Kim A, Hong E, Fisher BE, et al. Longitudinal associations between physical performance and cognition in individuals with Parkinson's disease. *Clinical Parkinsonism & Related Disorders*. (2025) 13:100370. doi: 10.1016/j.prdoa.2025.100370

58. Newman BT, Dhollander T, Reynier KA, Panzer MB, Druzgal TJ. Test–retest reliability and long-term stability of three-tissue constrained spherical deconvolution methods for analyzing diffusion MRI data. *Magn Reson Med*. (2020) 84:2161–73. doi: 10.1002/mrm.28242

59. Newman BT, Jacokes Z, Venkadesh S, Webb SJ, Kleinhans NM, McPartland JC, et al. Conduction velocity, G-ratio, and extracellular water as microstructural characteristics of autism spectrum disorder. *PLoS One*. (2024) 19:e0301964. doi: 10.1371/journal.pone.0301964

60. Newman BT, Patrie JT, Druzgal TJ. An intracellular isotropic diffusion signal is positively associated with pubertal development in white matter. *Dev Cogn Neurosci*. (2023) 63:101301. doi: 10.1016/j.dcn.2023.101301

61. Fischl B. FreeSurfer. *NeuroImage*. (2012) 62:774–81. doi: 10.1016/j.neuroimage.2012.01.021

62. Destrieux C, Fischl B, Dale A, Halgren E. Automatic parcellation of human cortical gyri and sulci using standard anatomical nomenclature. *NeuroImage*. (2010) 53:1–15. doi: 10.1016/j.neuroimage.2010.06.010

63. Veraart J, Novikov DS, Christiaens D, Ades-Aron B, Sijbers J, Fieremans E. Denoising of diffusion MRI using random matrix theory. *NeuroImage*. (2016) 142:394–406. doi: 10.1016/j.neuroimage.2016.08.016

64. Kellner E, Dhital B, Kiselev VG, Reisert M. Gibbs-ringing artifact removal based on local subvoxel-shifts. *Magn Reson Med*. (2016) 76:1574–81. doi: 10.1002/mrm.26054

65. Andersson JL, Sotiropoulos SN. An integrated approach to correction for off-resonance effects and subject movement in diffusion MR imaging. *NeuroImage*. (2016) 125:1063–78. doi: 10.1016/j.neuroimage.2015.10.019

66. Andersson JL, Graham MS, Zsoldos E, Sotiropoulos SN. Incorporating outlier detection and replacement into a non-parametric framework for movement and distortion correction of diffusion MR images. *NeuroImage*. (2016) 141:556–72. doi: 10.1016/j.neuroimage.2016.06.058

67. Andersson JL, Skare S, Ashburner J. How to correct susceptibility distortions in spin-echo echo-planar images: application to diffusion tensor imaging. *NeuroImage*. (2003) 20:870–88. doi: 10.1016/S1053-8119(03)00336-7

68. Greenspan H. Super-resolution in medical imaging. *Comput J*. (2009) 52:43–63.

69. Dhollander T, Connelly A. A novel iterative approach to reap the benefits of multi-tissue CSD from just single-shell (+ b= 0) diffusion MRI data. *Proc ISMRM*. (2016) 24:3010.

70. Dhollander T, Raffelt D, Connelly A. Towards interpretation of 3-tissue constrained spherical deconvolution results in pathology. *Proc Intl Soc Mag Reson Med*. (2017) 25:1815.

71. Mito R, Dhollander T, Xia Y, Raffelt D, Salvado O, Churilov L, et al. In vivo microstructural heterogeneity of white matter lesions in healthy elderly and Alzheimer's disease participants using tissue compositional analysis of diffusion MRI data. *NeuroImage: Clinical*. (2020) 28:102479. doi: 10.1016/j.nicl.2020.102479

72. Mito R, Dhollander T, Raffelt D. Investigating microstructural heterogeneity of white matter hyperintensities in Alzheimer's disease using single-shell 3-tissue constrained spherical deconvolution. *Proc Intl Soc Mag Reson Med*. (2018):135.

73. Kelly C, Dhollander T, Harding IH, Khan W, Beare R, Cheong JLY, et al. Brain tissue microstructural and free-water composition 13 years after very preterm birth. *NeuroImage*. (2022) 254:119168. doi: 10.1016/j.neuroimage.2022.119168

74. Raffelt D, Tournier JD, Rose S, Ridgway GR, Henderson R, Crozier S, et al. Apparent fibre density: a novel measure for the analysis of diffusion-weighted magnetic resonance images. *NeuroImage*. (2012) 59:3976–94. doi: 10.1016/j.neuroimage.2011.10.045

75. Hsu YC, Lo YC, Chen YJ, Wedeen VJ, Isaac Tseng WY. NTU-DSI-122: a diffusion spectrum imaging template with high anatomical matching to the ICBM-152 space. *Hum Brain Mapp*. (2015) 36:3528–41. doi: 10.1002/hbm.22860

76. Newman BT, Untaroiu A., Druzgal TJ (2020) *Proceedings of the ISMRM 28th General Meeting*. International Society for Magnetic Resonance in Medicine.

77. Raffelt DA, Tournier JD, Smith RE, Vaughan DN, Jackson G, Ridgway GR, et al. Investigating white matter fibre density and morphology using fixel-based analysis. *NeuroImage*. (2017) 144:58–73. doi: 10.1016/j.neuroimage.2016.09.029

78. Cruces RR, Royer J, Herholz P, Larivière S, Vos de Wael R, Paquola C, et al. Micapipe: A pipeline for multimodal neuroimaging and connectome analysis. *NeuroImage*. (2022) 263:119612. doi: 10.1016/j.neuroimage.2022.119612

79. Avants BB, Tustison N, Song G. Advanced normalization tools (ANTS). *Insight j*. (2009) 2:1–35.

80. Stikov N, Perry LM, Mezer A, Rykhlevskaia E, Wandell BA, Pauly JM, et al. Bound pool fractions complement diffusion measures to describe white matter micro and macrostructure. *NeuroImage*. (2011) 54:1112–21. doi: 10.1016/j.neuroimage.2010.08.068

81. Stikov N, Campbell JS, Stroh T, Campbell JSW, Lavelée M, Frey S, et al. In vivo histology of the myelin g-ratio with magnetic resonance imaging. *NeuroImage*. (2015) 118:397–405. doi: 10.1016/j.neuroimage.2015.05.023

82. Campbell JS, Leppert IR, Narayanan S, Campbell JSW, Boudreau M, Duval T, et al. Promise and pitfalls of g-ratio estimation with MRI. *NeuroImage*. (2018) 182:80–96. doi: 10.1016/j.neuroimage.2017.08.038

83. Mohammadi S, Callaghan MF. Towards in vivo g-ratio mapping using MRI: unifying myelin and diffusion imaging. *J Neurosci Methods*. (2021) 348:108990. doi: 10.1016/j.jneumeth.2020.108990

84. Rushton WAH. A theory of the effects of fibre size in medullated nerve. *J Physiol*. (1951) 115:101–22. doi: 10.1113/jphysiol.1951.sp004655

85. Berman S, Filo S, Mezer AA. Modeling conduction delays in the corpus callosum using MRI-measured g-ratio. *NeuroImage*. (2019) 195:128–39. doi: 10.1016/j.neuroimage.2019.03.025

86. Tournier JD, Smith R, Raffelt D, Tabbara R, Dhollander T, Pietsch M, et al. MRtrix3: a fast, flexible and open software framework for medical image processing and visualisation. *NeuroImage*. (2019) 202:116137. doi: 10.1016/j.neuroimage.2019.116137

87. Smith RE, Tournier JD, Calamante F, Connelly A. SIFT: spherical-deconvolution informed filtering of tractograms. *NeuroImage*. (2013) 67:298–312. doi: 10.1016/j.neuroimage.2012.11.049

88. Donahue EK, Foreman RP, Duran JJ, Jakowec MW, O'Neill J, Petkus AJ, et al. Increased perivascular space volume in white matter and basal ganglia is associated with cognition in Parkinson's disease. *Brain Imaging Behav*. (2023) 18:57–65. doi: 10.1007/s11682-023-00811-4

89. Donahue EK, Murdos A, Jakowec MW, Sheikh-Bahaei N, Toga AW, Petzinger GM, et al. Global and regional changes in perivascular space in idiopathic and familial Parkinson's disease. *Mov Disord*. (2021) 36:1126–36. doi: 10.1002/mds.28473

90. Ofori E, DeKosky ST, Febo M, Colon-Perez L, Chakrabarty P, Duara R, et al. Free-water imaging of the hippocampus is a sensitive marker of Alzheimer's disease. *NeuroImage: Clinical*. (2019) 24:101985. doi: 10.1016/j.nicl.2019.101985

91. Blair J C, Newman BT, Druzgal TJ "Evaluating lifespan tissue structure: comparing CSD signal fraction and VBM Grey matter density" *Proceedings of the ISMRM 27th General Meeting*. (2019)

92. Newman BT, Druzgal TJ "Diffusion microstructure measurements across the brain and lifespan" *Proceedings of the ISMRM 28th General Meeting*. (2022) 2739.

93. Perez Rodriguez Garcia G, Middlebrooks E, Mei S, Tsuboi T, Wong J, Burns M, et al. Functional and structural connectivity correlates of axial symptom outcomes after Pallidal deep brain stimulation in Parkinson's disease. *Brain Sci*. (2025) 15:1245. doi: 10.3390/brainsci15111245

94. Atkinson-Clement C, Pinto S, Eusebio A, Coulon O. Diffusion tensor imaging in Parkinson's disease: review and meta-analysis. *Neuroimage: Clinical*. (2017) 16:98–110. doi: 10.1016/j.nicl.2017.07.011

95. Fortin JP, Cullen N, Sheline YI, Taylor WD, Aselcioglu I, Cook PA, et al. Harmonization of cortical thickness measurements across scanners and sites. *NeuroImage*. (2018) 167:104–20. doi: 10.1016/j.neuroimage.2017.11.024

96. Owens-Walton C, Nir TM, Al-Bachari S. A worldwide study of white matter microstructural alterations in people living with Parkinson's disease. *npj Parkinsons Dis*. (2024) 10:151. doi: 10.1038/s41531-024-00758-3